Applied Catalysis B: Environmental 160–161 (2014) 534–541

Contents lists available at ScienceDirect

Applied Catalysis B: Environmental

journal homepage: www.elsevier.com/locate/apcatb

Ruthenium(0) nanoparticles stabilized by metal-organic framework (ZIF-8): Highly efficient catalyst for the dehydrogenation of dimethylamine-borane and transfer hydrogenation of unsaturated hydrocarbons using dimethylamine-borane as hydrogen source

Mehmet Yurderi[a], Ahmet Bulut[a], Mehmet Zahmakiran[a,*], Mehmet Gülcan[a], Saim Özkar[b]

[a] Department of Chemistry, Yüzüncü Yıl University, 65080 Van, Turkey
[b] Department of Chemistry, Middle East Technical University, 06800 Ankara, Turkey

ARTICLE INFO

Article history:
Received 7 April 2014
Received in revised form 2 June 2014
Accepted 6 June 2014
Available online 13 June 2014

Keywords:
Zeolitic imidazolate framework
Ruthenium nanoparticles
Dimethylamine-borane
Dehydrogenation
Transfer hydrogenation

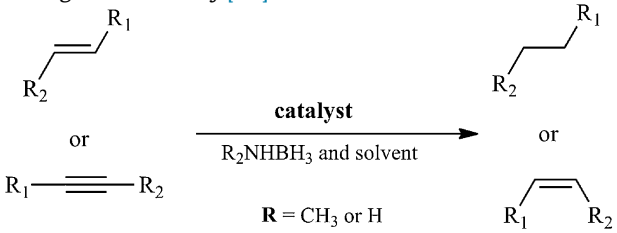
ABSTRACT

Ruthenium(0) nanoparticles supported on zeolitic imidazolate framework (ZIF-8), RuNPs/ZIF-8, were reproducibly prepared by borohydride reduction of $RuCl_3$/ZIF-8 precatalyst in water at room temperature. The characterization of the dehydrated RuNPs/ZIF-8 was done by a combination of complimentary techniques, which reveals that the formation of well-dispersed ruthenium(0) nanoparticles (1.9 ± 0.6 nm) on the surface of ZIF-8 by keeping the host framework intact. The catalytic activity of RuNPs/ZIF-8 was firstly tested in the dehydrogenation of dimethylamine-borane ($(CH_3)_2NHBH_3$) in toluene. We found that ruthenium(0) nanoparticles supported on ZIF-8 can catalyze the dehydrogenation of dimethylamine-borane with an initial TOF value of 59 min^{-1} at 40 °C. Additionally, RuNPs/ZIF-8 catalyze the transfer hydrogenation of various unsaturated substrates in the presence of dimethylamine borane as hydrogen source even at low catalyst loadings. More importantly, they show high durability against leaching and sintering throughout the catalytic runs, which make them reusable catalyst in these important catalytic transformations.

© 2014 Elsevier B.V. All rights reserved.

1. Introduction

In the past decade, there has been growing attention in the metal catalyzed dehydrogenation of ammonia-borane (NH_3BH_3) and its homologs ($MeNH_2BH_3$, $(Me)_2NHBH_3$, *etc.*) [1,2] due to the current interest in the hydrogen storage, which is still one of the key problems in the "Hydrogen Economy" [3–5]. Additionally, the importance of catalytic dehydrogenation of amine-borane adducts in the polymer synthesis [6,7], tandem dehydrogenation–hydrogenation [8,9], and transfer hydrogenation [10] has also made a prominent contribution to the progress in this field. Of particular importance are the results of recent studies [viii-x] revealing that amine-boranes can be used as easily transportable sources of hydrogen for the catalytic hydrogenation of C–C multiple bonds (**1**), which is one of the most important processes in the organic chemistry [11].



Although [Pd(SIPr)(PCy_3)] [ix] and [$ReBr_2$(NO)(P^iPr_3)(H_2)] [x] complexes have been reported to provide notable activity in these reactions, their difficult separation from the reaction mixture and requirement of ligands/additives hinder their use in practical applications. At this concern, because of the advantages of nanocatalysis [12], the current research has been directed toward the development of metal nanoparticles (NPs) possessing high activity in the tandem dehydrogenation/hydrogenation reactions. Manners has reported that Rh(0) NPs formed *in-situ* from the reduction of [Rh(1,5-cod)Cl)]$_2$ can catalyze the tandem dimethylamine-borane

* Corresponding author. Tel.: +90 5323034741; fax: +90 432 225 18 02.
E-mail addresses: mzahmakiran@gmail.com, zmehmet@yyu.edu.tr (M. Zahmakiran).

http://dx.doi.org/10.1016/j.apcatb.2014.06.009
0926-3373/© 2014 Elsevier B.V. All rights reserved.

dehydrogenation/alkene hydrogenation even at room temperature [viii]. However, since the sole stabilizer present in the system is the weakly coordinating chloride anion, which cannot provide enough stabilization for Rh(0) NPs [13] they cannot be used as active catalyst for the second run resulting from their aggregation into the bulk. Actually, the fabrication of metal nanoparticles with high stability against to agglomeration throughout their catalytic use has great importance in nanocatalysis as their aggregation into bulk form leads to a momentous decrease in their catalytic activity [xiii]. In this context, the generation of the metal nanoparticles within the framework of porous materials has already been acknowledged for preventing aggregation of metal nanoparticles [12,14]. Of particular interest, metal organic frameworks (MOFs), which are highly crystalline hybrid materials and combined from metal ions and rigid organic ligands, can be employed as host materials for the stabilization of ligand-free metal nanoparticles [15]. MOFs provide high specific surface areas and tunable pore sizes by appropriate combination of structural subunits during their synthesis, which is the most important advantage of these materials with respect to silica and carbon based support materials used for the same purpose [16].

Herein we report the synthesis, characterization and catalytic employment of ruthenium(0) nanoparticles supported on zeolitic imidazolate framework (ZIF-8; $[Zn(MeIM)_2]_n$) hereafter referred to as RuNPs/ZIF-8, in the dehydrogenation of dimethylamine-borane ($(CH_3)_2NHBH_3$; DMAB) and tandem dimethylamine-borane dehydrogenation/olefin hydrogenation in toluene at 40 °C. ZIF-8 was selected as representative microporous metal–organic framework, which has stable intersecting three-dimensional structure that possesses large surface area (1400 $m^2\,g^{-1}$) and high thermal stability (>500 °C) [17]. Up to date, ZIF-8 has been used as support materials for Ir [18], Au [19], Ag [20], Ni [21], Pd [22], Pt [23], and ZnO [24] nanoparticles.

RuNPs/ZIF-8 was reproducibly prepared through the conventional impregnation followed by subsequent reduction method in water at room temperature and dehydration by heating to 300 °C under vacuum (10^{-3} Torr). The characterization of the resulting material by using inductively coupled plasma-optical emission spectroscopy (ICP-OES), powder X-ray diffraction (P-XRD), X-ray photoelectron spectroscopy (XPS), Raman spectroscopy, conventional transmission electron microscopy (CTEM), high resolution-TEM (HRTEM) and N_2-adsorption–desorption technique reveals that the formation of well-dispersed 1.9 ± 0.6 nm RuNPs on the surface of ZIF-8 without distorting the host material framework. These supported RuNPs were found to be highly active catalyst in the dehydrogenation of dimethylamine-borane and transfer hydrogenation of unsaturated hydrocarbons (alkenes, alkynes) in toluene at 40 °C. In addition to their high activity, they also show high stability against leaching and sintering throughout the catalytic runs, which make them highly reusable catalyst for these catalytic transformations.

2. Experimental

2.1. Materials

ZIF-8 ($[Zn(MeIM)_2]_n$), dimethylamine-borane ($(CH_3)_2NHBH_3$), ruthenium(III) chloride trihydrate ($RuCl_3{\cdot}3H_2O$), sodium borohydride ($NaBH_4$), deuterated NMR solvents and all organic substrates were purchased from Sigma-Aldrich®. Dimethylamine-borane was purified by sublimation at 25 °C. All glassware and Teflon coated magnetic stir bars were cleaned with acetone, followed by copious rinsing with distilled water before drying in an oven at 150 °C. All reactions and manipulations were performed under an atmosphere of dry nitrogen using standard Schlenk technique or in a glove-box filled with dry argon unless otherwise specified.

2.2. Characterization

Ruthenium content of the samples was determined by ICP-OES (Leeman, Direct Reading Echelle) after each sample was completely dissolved in a mixture of HNO_3/HCl (1/3 ratio). Powder X-ray diffraction (XRD) patterns were recorded with a MAC Science MXP 3TZ diffractometer using Cu-Kα radiation (wavelength 1.54 Å, 40 kV, 55 mA). CTEM and HRTEM samples were prepared by dropping one drop of dilute suspension on copper coated carbon TEM grid and the solvent was then dried. The conventional TEM was carried out on a JEOL JEM-200CX transmission electron microscopes operating at 120 kV. HRTEM was run on a JEOL JEM-2010F transmission electron microscope operating at 200 kV. The XPS analyses were performed on a Physical Electronics 5800 spectrometer equipped with a hemispherical analyzer and using monochromatic Al-Kα radiation (1486.6 eV, the X-ray tube working at 15 kV and 350 W, and pass energy of 23.5 eV). The Raman spectra of samples were recorded on Bruker RFS-100/S series Raman spectrometer equipped with Nd-YAG laser at 1064 nm using the FT-Raman technique. The progress of the reaction was followed by GC analysis of samples drawn from the reaction solution. All of the GC analyses were performed on a TRB-WAX column (30 m × 0.25 mm × 0.25 mm) with a Shimadzu GC-2010 equipped with a FID detector. NMR spectra were recorded on Bruker Avance DPX 400 MHz spectrometer (400.1 MHz for ^{1}H NMR; 128.2 MHz for ^{11}B NMR). Tetramethylsilane was used as the internal reference for ^{1}H NMR chemical shifts. $BF_3{\cdot}(C_2H_5)_2O$ was used as the external reference for ^{11}B NMR chemical shifts.

2.3. Preparation of Ruthenium(0) nanoparticles supported on zeolitic imidazolate framework (RuNPs/ZIF-8)

Prior to ruthenium precursor ($RuCl_3{\cdot}3H_2O$) loading, ZIF-8 was immersed in methanol under ambient conditions for 48 h. Then, ZIF-8 powders were isolated by suction filtration and the isolated ZIF-8 sample was evacuated at room temperature for over 8 h, then at 250 °C for 4 h. Next, in a 20 mL round-bottom flask, ZIF-8 (200 mg) was added to a solution of $RuCl_3{\cdot}3H_2O$ (11 mg, 0.04 mmol) in 10 mL of water ([Ru] = 1.99 mM). This slurry was stirred with a rate of 700 rpm at room temperature for 6 h. The mixture was filtered by suction filtration using Whatman-1 filter paper and washed three times with 20 mL of deionized water and dried in oven at 100 °C. The ruthenium content of the resulting sample was determined by ICP-OES analysis. Then, 100 mg $RuCl_3$/ZIF-8 (containing 1.12 wt% Ru corresponds to 0.01 mmol Ru) was added into a fresh 5.0 mL aqueous solution of $NaBH_4$ (3.8 mg, 0.1 mmol $NaBH_4$) and the resulting solution was stirred for half an hour under air at room temperature. After centrifugation (6000 rpm, 5 min.), copious washing with water (3 × 20 mL), filtration, and drying in oven at 100 °C, RuNPs/ZIF-8 was obtained as dark gray powder. RuNPs/ZIF-8 in powder form was put into a quartz tube which was placed in furnace and connected to vacuum (10^{-3} Torr). Thus the sample was dehydrated with the following heating schedule, using a temperature controller: 0.5 h from 25 to 100 °C, 1 h at 100 °C, 4 h from 100 to 300 °C and 4 h at 300 °C. After thermal treatment, the sample inside the quartz tube was cooled down to room temperature, sealed and transferred into the glove box.

2.4. RuNPs/ZIF-8 catalyzed dehydrogenation of dimethylamine-borane

The catalytic activity of RuNPs/ZIF-8 in the dehydrogenation of dimethylamine-borane was determined by measuring the rate of

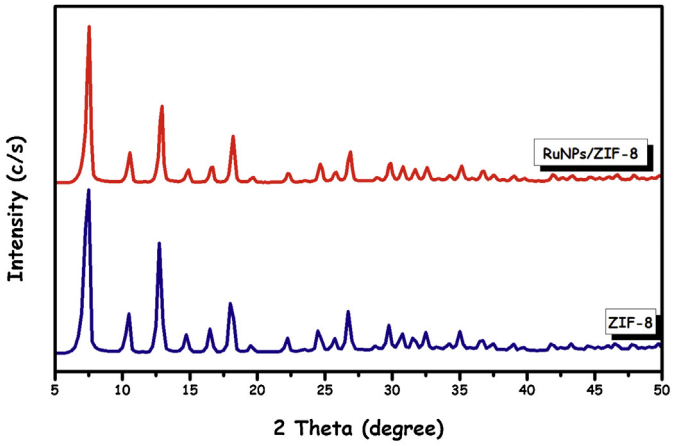


Fig. 1. The powder X-ray diffraction (P-XRD) patterns of ZIF-8 and RuNPs/ZIF-8.

hydrogen generation. The volume of released gas during the reaction was monitored using the gas burette by water displacement. In a glovebox, a 25 mL jacketed one-necked reaction flask containing a septum Teflon-coated stir bar was charged with 90 mg RuNPs/ZIF-8 (10 μmol Ru corresponds to % 1 mol catalyst) and 8 mL toluene. It was then sealed, brought outside of the glovebox and placed on a magnetic stirrer (Heidolph MR-3004). The reaction flask was thermostated to 40 °C by circulating water through its jacket from a constant temperature bath (Lab Companion RW-0525) and the mixture was stirred for 15 min to achieve thermal equilibrium. Next, 2 mL toluene solution of $(CH_3)_2NHBH_3$ (1 mmol) was added into the reaction tube via its septum by using a 5 mL gastight syringe and the catalytic reaction was started (t = 0 min) by stirring the mixture at 700 rpm.

2.5. RuNPs/ZIF-8 Catalyzed Transfer Hydrogenation of alkenes

In an argon filled glovebox, $(CH_3)_2NHBH_3$ (1 mmol), unsaturated substrate (1 mmol) and a catalytic amount of RuNPs/ZIF-8 (0.02 mmol, 1 mol% Ru) were dissolved in toluene-d_8 (2 mL) in a screw-cap vial. The vial was sealed and placed into an oil bath (40 °C), and the mixture was stirred at 700 rpm for 16 h. The contents of vial were analyzed by GC, ^{1}H and ^{11}B NMR spectroscopy.

3. Results and discussion

RuNPs/ZIF-8 was prepared as a new catalytic material by a procedure comprising of solution phase impregnation of $RuCl_3$ on ZIF-8 support, the reduction of Ru^{3+} ions with sodium borohydride *([$NaBH_4$]/[Ru] was kept at 10 to ensure complete reduction of Ru^{3+} to Ru^0)* in an aqueous solution all at room temperature, then dehydration of RuNPs/ZIF-8 by gradual heating to 300 °C. The resulting RuNPs/ZIF-8 was isolated as gray powder and characterized by inductively coupled plasma optical emission spectroscopy (ICP-OES) and powder X-ray diffraction (P-XRD). The P-XRD pattern of RuNPs/ZIF-8 (containing 1.12 wt% Ru as determined by ICP-OES) is identical with that of ZIF-8 (Fig. 1). The absence of Bragg peaks assignable to other phases or impurities is revealing that the host material ZIF-8 remains intact at the end of the preparation protocol. The slight decrease in the intensity of Bragg peaks in RuNPs/ZIF-8 can be explained by the changes in the charge distribution and electrostatic fields as a result of the existence of ruthenium(0) nanoparticles on the surface and interaction of their electrophilic surface with framework atoms.

X-Ray photoelectron spectroscopy (XPS) provides further insights to the oxidation state of ruthenium and surface composition of the resulting RuNPs/ZIF-8. The survey scan XPS spectrum

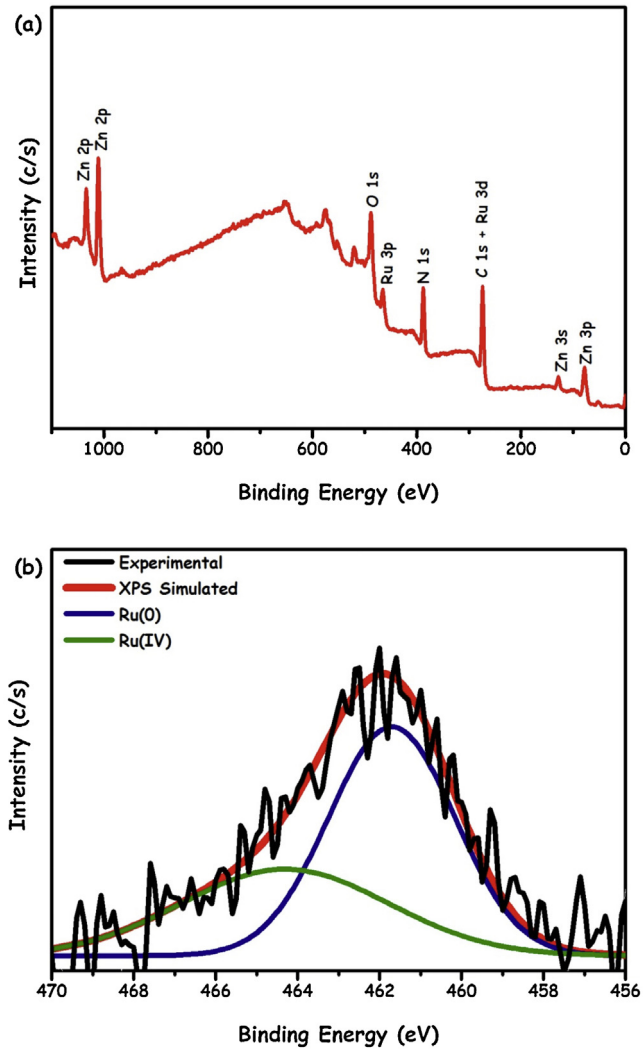


Fig. 2. (a) Survey scan XPS spectrum of the RuNPs/ZIF-8 and (b) high resolution Ru 3p XPS spectrum of the RuNPs/ZIF-8.

of the RuNPs/ZIF-8 sample is depicted in Fig. 2(a), which shows the presence of the ZIF-8 framework elements (Zn, C, N) and Ru. Unfortunately, the overlap of the C 1s and Ru $3d_{3/2}$ peaks around 284 eV makes it difficult to correctly analyze this region for ruthenium. Therefore, only the Ru $3p_{3/2}$ peak (Fig. 2(b)) had to be used for the ruthenium analysis. The deconvolution of high resolution Ru 3p XPS spectrum of the RuNPs/ZIF-8 sample gives a distinctive peak at 461.6 eV that can readily be assigned to Ru(0) $3p_{3/2}$ [25]. The peak observed at 463.5 eV reveals the presence of RuO_2, which may originate from the surface oxidation of ruthenium(0) nanoparticles during the XPS sampling procedure [26]. In addition to XPS, we also performed Raman analysis on RuNPs/ZIF-8 to check whether RuO_2 is really formed during the XPS sampling procedure or in the preparation of RuNPs/ZIF-8. It was observed that the characteristics Raman peaks of RuO_2 in the range 400–1200 cm^{-1} [xxvi] were missing in the Raman spectrum of RuNPs/ZIF-8, which confirms that the detection of RuO_2 by XPS is resulting from the surface oxidation of ruthenium(0) nanoparticles during the XPS sampling procedure.

Nitrogen adsorption–desorption isotherms of ZIF-8 and RuNPs/ZIF-8 are given in Fig. 3 and they show type I shape, which is a characteristic of microporous materials [27]. The micropore volume and area were determined for ZIF-8 and RuNPs/ZIF-8 by the t-plot method [28]. The appreciable decrease in the micropore

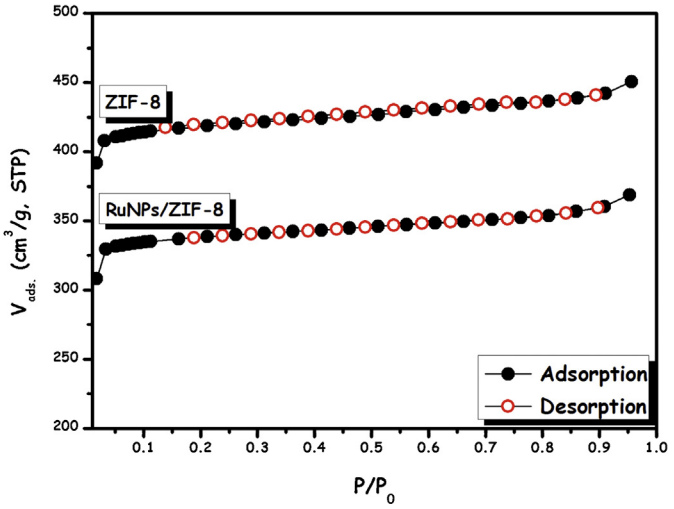


Fig. 3. Nitrogen adsorption–desorption isotherms of ZIF-8 and RuNPs/ZIF-8.

volume (from 0.668 to 0.598 $cm^3\,g^{-1}$) and the BET surface area (from 1651 to 1454 $m^2\,g^{-1}$) on passing from ZIF-8 to RuNPs/ZIF-8 can be explained by blocking of the windows of cavities by the deposition of ruthenium(0) nanoparticles exist on the surface as the electron microscopy analyzes (*vide infra*) show the existence of ruthenium(0) nanoparticles supported on the surface of ZIF-8.

The conventional transmission electron microscopy (CTEM) and high resolution transmission electron microscopy (HRTEM) were performed for the size and morphology analyses of RuNPs/ZIF-8. The bright field CTEM image of RuNPs/ZIF-8 sample with a ruthenium loading of 1.12% wt is given in Fig. 4(a), which reveals the presence of well dispersed ruthenium(0) nanoparticles on the surface of ZIF-8. The mean diameter of these ZIF-8 supported ruthenium(0) nanoparticles was found to be 1.9 ± 0.6 nm (Fig. 4(b)). HRTEM image of RuNPs/ZIF-8 given in Fig. 4(c) indicates that the highly crystalline feature of the particles with a crystalline spacing of 0.21 nm, which agrees with the (101) lattice spacing of ruthenium [29].

The catalytic activity of RuNPs/ZIF-8 with various ruthenium concentrations was investigated in the dehydrogenation of DMAB at 40 °C to determine the effect of ruthenium concentration on the dehydrogenation rate. Fig. 5(a) shows mol H_2/mol DMAB versus time graph for the RuNPs/ZIF-8 catalyzed dehydrogenation of DMAB at 40 °C for different ruthenium concentrations. An almost linear hydrogen evolution starts immediately as the preformed catalyst was used. The rate of hydrogen generation was determined from the linear portion of the plot for each experiment. Expectedly, the hydrogen generation rate increases by the increase of ruthenium concentrations (k_{obs} = 0.25, 0.3, 0.4 and 0.55 mol H_2/(mol DMAB)(h) for [Ru] = 0.50, 0.75, 1.00 and 1.25 mM, respectively). The plot of hydrogen generation rate versus catalyst concentration, both on logarithmic scales, gives a straight line with a slope of 1.24 as shown in Fig. 5(b). This result, within the experimental error, indicates that RuNPs/ZIF-8 catalyzed dehydrogenation of DMAB is first order with respect to the ruthenium concentration.

RuNPs/ZIF-8 catalyzed dehydrogenation of DMAB was also carried out at different temperatures in the range 40–60 °C to investigate the effect of temperature on the hydrogen generation rate. Fig. 6(a) gives the plot of mol of H_2/mol DMAB versus time graph for the dehydrogenation of DMAB catalyzed by RuNPs/ZIF-8 at constant [DMAB] and [Ru] concentrations for various temperatures. As seen from this graph the rate of dehydrogenation increases by the increase of the temperature, RuNPs/ZIF-8 provide *initial* TOF values of 59, 68, 82, 121, and 151 min^{-1} at 40, 45, 50, 55 and 60 °C, respectively. The values of rate constant *k* determined from the

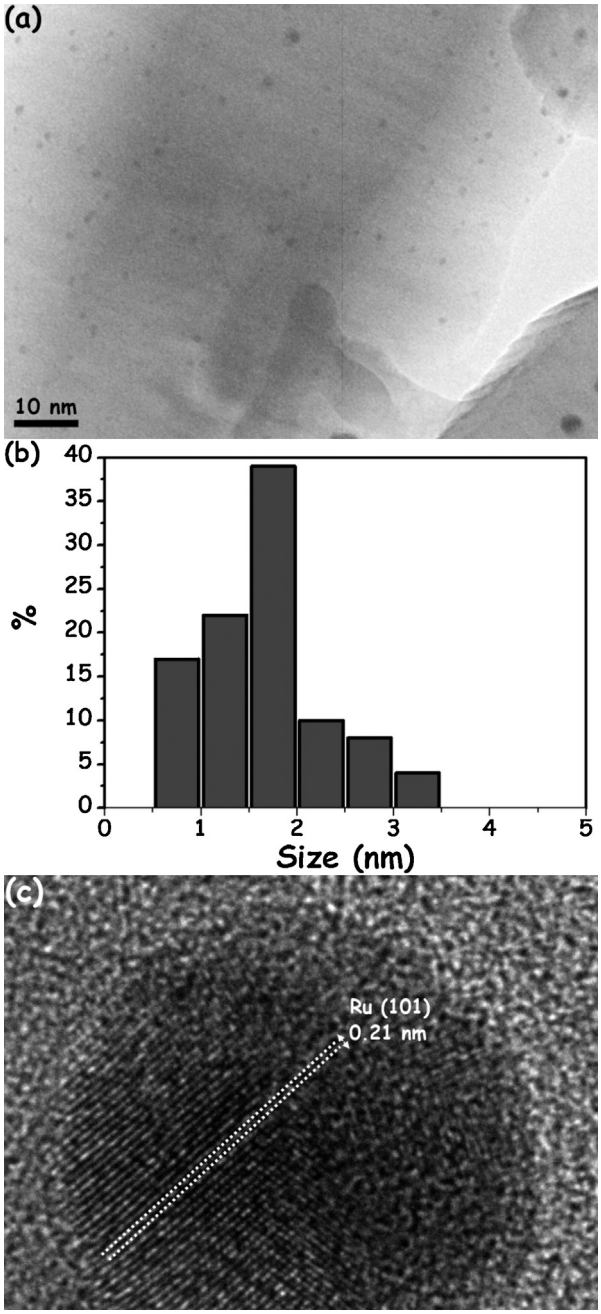


Fig. 4. (a) TEM image and corresponding size histogram (inset) of RuNPs/ZIF-8, (b) TEM and high resolution TEM (inset) images of RuNPs/ZIF-8.

linear portion of the mol of H_2/mol DMAB versus time plot at five different temperatures were used for Arrhenius plot (Fig. 6(b)) to calculate Arrhenius activation energy (Ea = 42.5 kJ/mol). This activation energy value is remarkably lower than that of the previously reported best heterogeneous catalyst ($PdNPs@Cu_3(btc)_2$; Ea = 174 kJ/mol) [30] for the dehydrogenation of DMAB but slightly higher than that of found by Rh NPs (Ea = 34 kJ/mol) [31]. The uniqueness of RuNPs/ZIF-8 catalyst among the different supported ruthenium nanoparticles was also tested by using the most commonly used solid support materials (SiO_2, Al_2O_3 and C) in the dehydrogenation of DMAB under the identical conditions (in toluene at 40 °C). The *initial* TOF values were found to be 4, 6, and 9 min^{-1} with the generation of <0.15 equiv. of H_2 for RuNPs/SiO_2, RuNPs/Al_2O_3 and RuNPs/C catalysts, respectively. The low activity and conversion values obtained by these support materials can

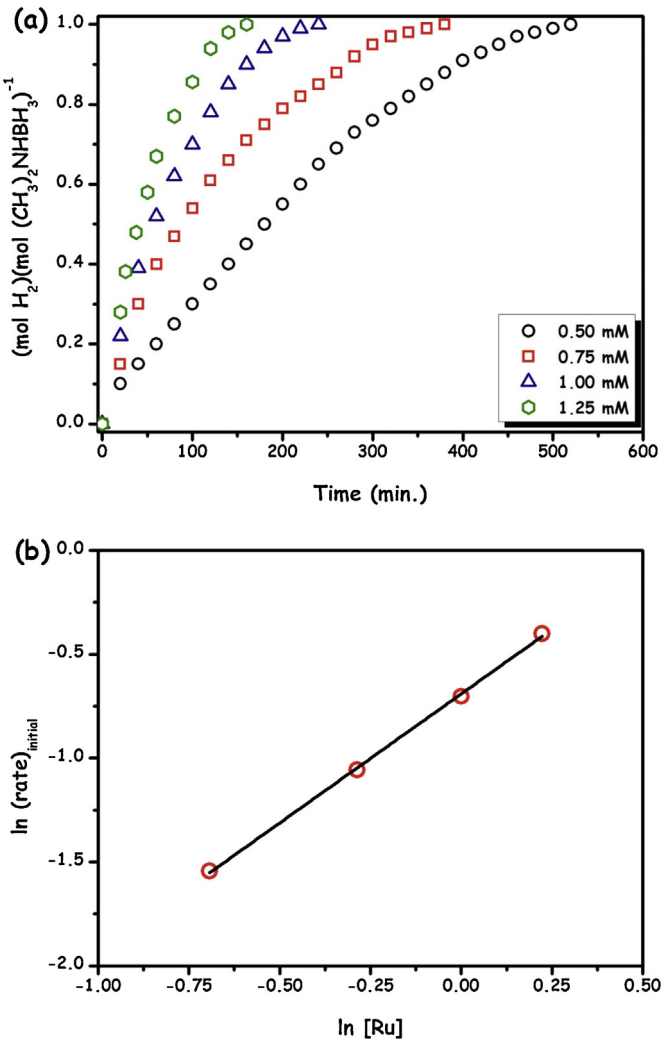


Fig. 5. (a) Plot of mol H_2/mol $(CH_3)_2NHBH_3$ vs time (min.), (b) Plot of hydrogen generation rate versus the catalyst concentration (both in logarithmic scale; $y = -10.69 + 1.24x$) for RuNPs/ZIF-8 catalyzed dehydrogenation of DMAB in different ruthenium concentrations at 25 °C.

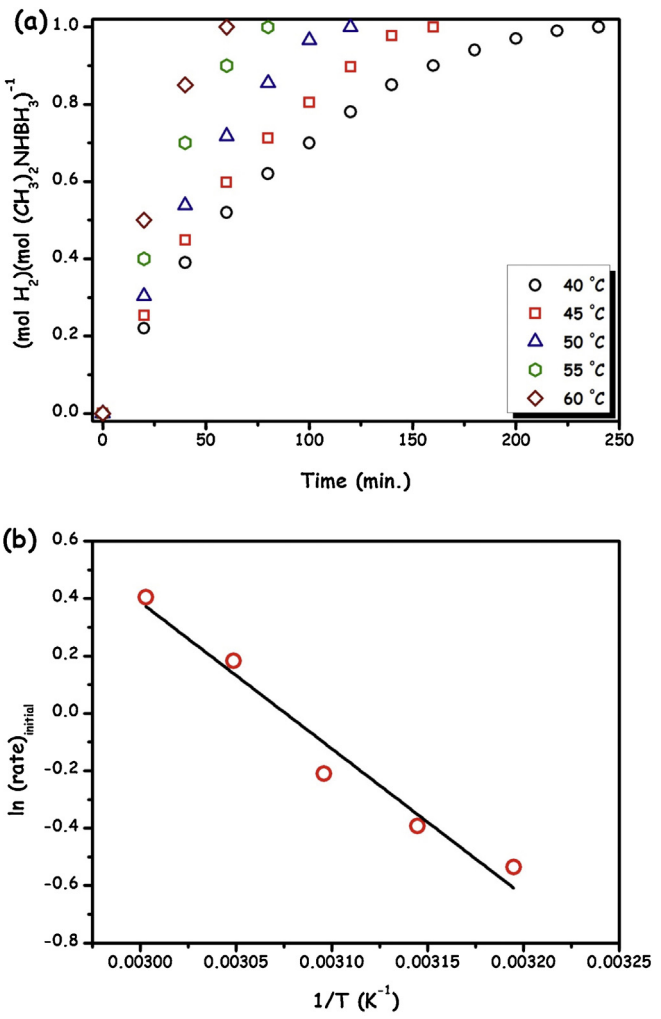
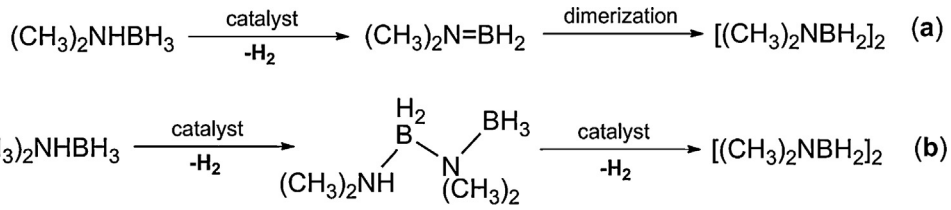


Fig. 6. (a) Plot of mol H_2/mol $(CH_3)_2NHBH_3$ vs time (min), (b) Arrhenius plot ($y = 15.72 - 5112x$) for RuNPs/ZIF-8 catalyzed dehydrogenation of DMAB at different temperatures.

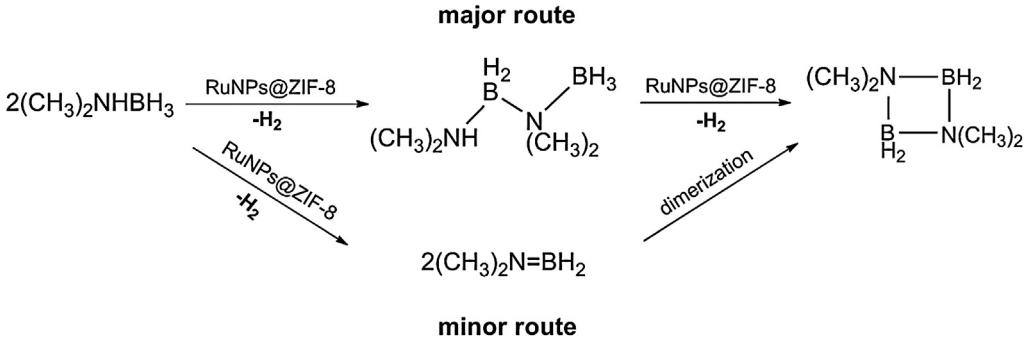
be explained by the agglomeration of surface bound ruthenium nanoparticles during the dehydration step, should be done as the existence of trace of amount of water in the reaction medium shifts the reaction to the hydrolysis of DMAB [32]. TEM images of these catalysts (Fig. SI-2) clearly indicates the surface clumping of ruthenium nanoparticles which form large sized agglomerated particles. The interaction between ZIF-8 framework and surface bound ruthenium nanoparticles might be strong enough to prevent the surface agglomeration of these particles. Understanding the existing synergistic effects between the metal and ZIF-8 support remains an active area of research in our group.

We further tested the durability of RuNPs/ZIF-8 catalyst by performing the dehydrogenation of DMAB in toluene at 40 °C and recovering RuNPs/ZIF-8 from the reaction solution after the completion of first run for the next round of reaction. These reusability experiments showed that RuNPs/ZIF-8 preserved > 85% of its initial activity after fifth catalytic run (Fig. 7(a)). RuNPs/ZIF-8 sample harvested from the fifth catalytic run was analyzed by ICP-OES, P-XRD and CTEM. The sum of their results showed that no obvious changes in Ru loading, ZIF-8 crystallinity and RuNPs morphology (Fig. SI-2). The slight decrease in the activity of RuNPs/ZIF-8 can be attributed to increase in the average size of RuNPs from 1.9 ± 0.6 nm to 3.1 ± 0.9 nm (Fig. 7(b)). These results indicate that RuNPs/ZIF-8 was stable under the current DMAB dehydrogenation conditions and could be reused for multiple runs of the dehydrogenation of DMAB. Moreover, the reusability performance of RuNPs/ZIF-8 (retaining > 85% activity) is better than that of previously reported Pd [xxx], Rh [viii,xxxi] and Ru [33,34] nanoparticles tested in the same reaction.

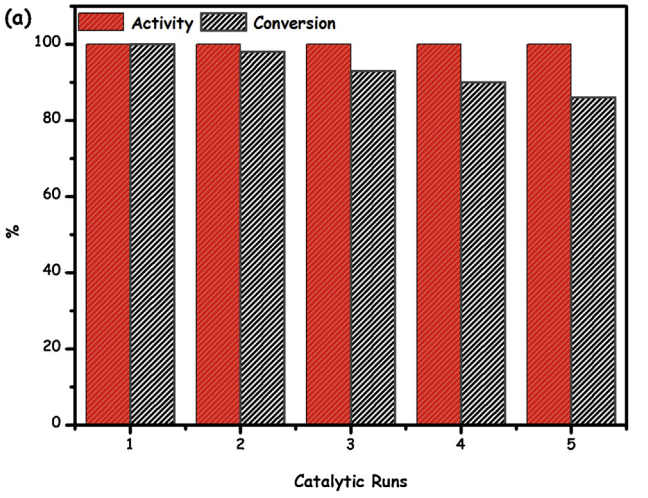
The progress of RuNPs/ZIF-8 catalyzed dehydrogenation of DMAB was also monitored by ^{11}B NMR spectroscopy to gain some mechanistic insights. The previous mechanistic studies have shown that two pathways (Scheme 1) are possible for the metal catalyzed dehydrogenation of DMAB [35–40]. In the mechanism **a**, hydrogen release takes place on the metal surface to produce two molecules of $(CH_3)_2N{=}BH_2$, which subsequently dimerizes to produce $[(CH_3)_2NBH_2]_2$. In the case of mechanism **b**, hydrogen release occurs in two separate steps, both of them occur at the metal center. In the first step, one equiv. of H_2 is lost in an intermolecular way to form $[(CH_3)_2NH\text{-}BH_2\text{-}N(CH_3)_2\text{-}BH_3]$, with a following intramolecular route releasing an additional equiv. of H_2 and forming $[(CH_3)_2NBH_2]_2$ [xxxv-xl]. Although the mechanism **a** has been widely accepted, the mechanism **b** has been postulated for the dehydrogenation of DMAB at elevated temperatures (≥40 °C) [41]. It has also been reported that in some systems most notably Ru-based systems both of these mechanisms can operate in parallel [42].



Scheme 1. The possible mechanisms for the metal catalyzed dehydrogenation of DMAB.



Scheme 2. The proposed mechanism for the RuNPs/ZIF-8 catalyzed dehydrogenation of DMAB in toluene at 40 °C.



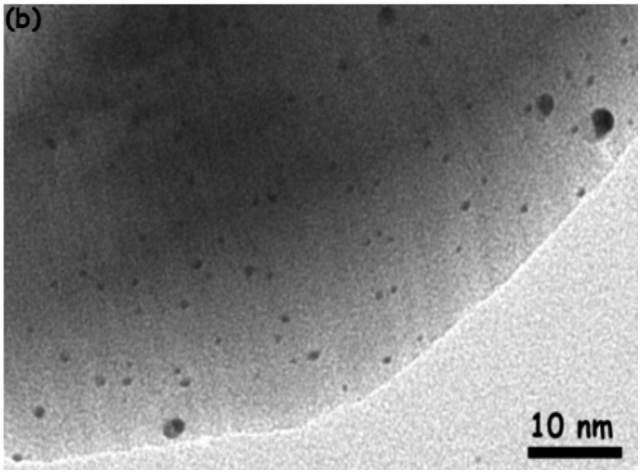


Fig. 7. (a) The percentage of conversion and retained catalytic activity of RuNPs/ZIF-8 in the successive catalytic runs for the dehydrogenation of DMAB at 40 °C and (b) CTEM image of RuNPs/ZIF-8 harvested after the fifth catalytic run of the dehydrogenation of DMAB.

Fig. 8 depicts ^{11}B-{^{1}H}-NMR spectra recorded from the reaction solution at different reaction times. The inspection of NMR spectra indicates the presence of two intermediates $(CH_3)_2N{=}BH_2$ (δ = 37 ppm, t, $J_{B\text{-}H}$ = 130 Hz) and $[(CH_3)_2NH\text{-}BH_2\text{-}N(CH_3)_2\text{-}BH_3]$ (δ = 1 ppm, t, $J_{B\text{-}H}$ = 106 Hz) formed during the conversion of $(CH_3)_2NHBH_3$ (δ = −14 ppm, q, $J_{B\text{-}H}$ = 95 Hz) to $[(CH_3)_2NBH_2]_2$ (δ = 6 ppm, t, $J_{B\text{-}H}$ = 112 Hz). This observation supports the point that RuNPs/ZIF-8 catalyzed dehydrogenation of DMAB occurs through both of two mechanisms. These two intermediates then yield the product in different routes; through dimerization of $(CH_3)_2N{=}BH_2$ or metal catalyzed intramolecular H_2 release for $[(CH_3)_2NH\text{-}BH_2\text{-}N(CH_3)_2\text{-}BH_3]$. However, the observation of $[(CH_3)_2NH\text{-}BH_2\text{-}N(CH_3)_2\text{-}BH_3]$ signal in higher fraction and for longer time than the signal of $(CH_3)_2N{=}BH_2$ indicates that the mechanism **b** is the major route for the RuNPs/ZIF-8 catalyzed dehydrogenation of DMAB (Scheme 2).

RuNPs/ZIF-8 was also tested as catalyst in the transfer hydrogenation of unsaturated hydrocarbons by using DMAB as hydrogen

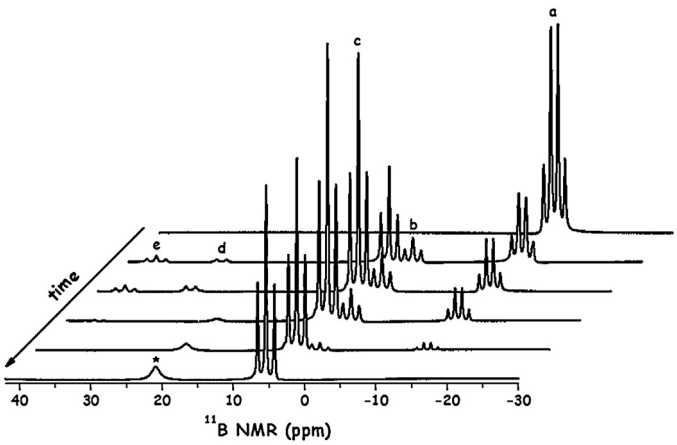
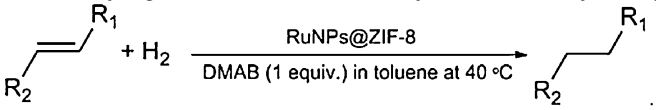
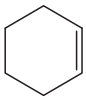
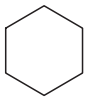
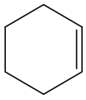
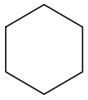
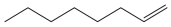
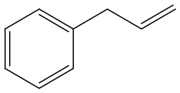
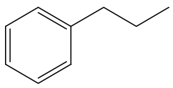
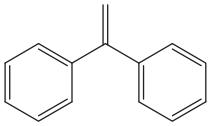
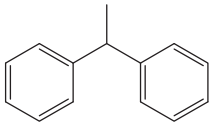
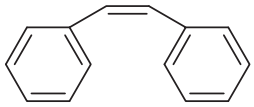


Fig. 8. ^{11}B NMR spectra of the reaction solution taken at different reaction times during the dehydrogenation of DMAB catalyzed by RuNPs/ZIF-8 in toluene at 40 °C; (a) $(CH_3)_2NHBH_3$, (b) $(CH_3)_2NH\text{-}BH_2\text{-}N(CH_3)_2\text{-}BH_3$, (c) $[(CH_3)_2NBH_2]_2$, (d) $HB(N(CH_3)_2)_2$, (e) $(CH_3)_2N{=}BH_2$ and * shows borate resonance result from exposure of the sample to air.

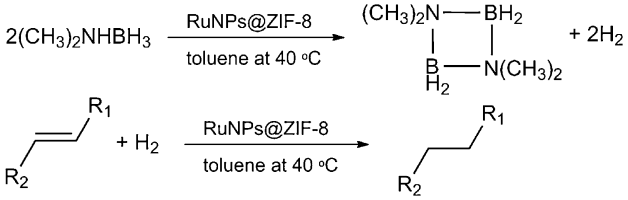
Table 1
Transfer hydrogenation of unsaturated hydrocarbons catalyzed by RuNPs/ZIF-8 using DMAB as hydrogen source in toluene at 40 °C.



Entry	Substrate	Product	Dehyrogenation[a] (%)	Hydrogenation[b] (%)
1			100	>98
2[c]			97	>92
3			100	>99
4			100	>99
5			100	>97
6			100	>97

[a] Determined by the integration of ^{11}B NMR spectra.
[b] Determined by GC analyses.
[c] For the 5th catalytic reuse.

source. In a typical experiment $(CH_3)_2NHBH_3$ (1 equiv.), cyclohexene (1 equiv.) and RuNPs/ZIF-8 (1 mol% Ru) were added into toluene-d_8 in a screw-cap vial under Ar atmosphere. The mixture was stirred for 12 h at 40 °C and the content was analyzed by GC and NMR spectroscopy. The sum of their results reveals the complete conversion of $(CH_3)_2NHBH_3$ to $[(CH_3)_2NBH_2]_2$ and cyclohexene to cyclohexane. A control experiment starting with DMAB and cyclohexene was performed in the absence of RuNPs/ZIF-8 under the identical conditions and showed no product of dehydrogenation/hydrogenation reactions. Additionally, (*i*) hydroboration of alkene was not observed in ^{11}B NMR spectrum taken from the solution at the end of experiment and (*ii*) the complete reduction of cyclohexene to cyclohexane in the presence of RuNPs/ZIF-8 could be achieved by using 1 bar external H_2 pressure within 2 h. RuNPs/ZIF-8 was shown to efficiently catalyze the transfer hydrogenation of a range of unsaturated hydrocarbons by using DMAB as a H_2 source at low catalyst loading (1% mol Ru) and 40 °C and representative results are listed in Table 1.



RuNPs/ZIF-8 can also act as reusable catalyst in the transfer hydrogenation of olefins. For example, when RuNPs/ZIF-8 are reused in the transfer hydrogenation of cyclohexene they retains almost their inherent activity at the fifth catalytic run with quantitative conversion (>92%) (Entry 2 in Table 1). The slight drop in the activity of RuNPs/ZIF-8 can be explained by the increase in the size of RuNPs as evidenced by CTEM analyses of RuNPs/ZIF-8 sample harvested from the fifth catalytic run of DMAB dehydrogenation (*vide supra*). RuNPs/ZIF-8 catalyzes the transfer hydrogenation of not only cyclic substrates but also acyclic substrates. As an example, 1-octene was quantitatively converted to octane (Entry 3 in Table 1). The transfer hydrogenation of alkynes to alkenes was also catalyzed by RuNPs/ZIF-8 in the presence of DMAB. For example, diphenylethyne was converted to to stilbene in high yield when 2 equivalents DMAB per mole of alkyne used in the presence of RuNPs/ZIF-8 catalyst (Entry 6 in Table 1). The hydrogenation of substrate likely occurs through an associative mechanism consisting of three steps: (*i*) alkene adsorption on the surface of the hydrogenated RuNPs/ZIF-8, (*ii*) hydrogen migration to the alkene unsaturated bond, and finally (*iii*) reductive elimination of the free alkane [43].

The present system is "relatively green" in terms of its environmental impact as it satisfies the major parts of the green chemistry requirements [44] including the followings: (*i*) it is 100% selective and minimizes by products or waste; (*ii*) it maximizes the incorporation of all reactants into the products; (*iii*) it requires relatively low energy as it occurs under mild condition; (*iv*) it is catalytic, not stoichiometric; (*v*) real-time monitoring is easy by measuring the H_2 uptake, ^1H NMR, or GC analysis, for example.

4. Conclusions

In the current work, ruthenium(0) nanoparticles supported on zeolitic imidazolate framework (RuNPs/ZIF-8) were synthesized, characterized and employed as catalyst in the dehydrogenation of dimethylamine-borane and transfer hydrogenation of unsaturated hydrocarbons (alkenes and alkynes) in the presence of dimethylamine-borane as hydrogen source. Some of the major findings of the current study can be summarized as follows:

(a) RuNPs/ZIF-8 was prepared, for the first time, by using a simple and reproducible procedure. The characterization of new catalytic materials was done by a combination of complimentary techniques, which revealed that the formation of well-dispersed ruthenium(0) nanoparticles (1.9 ± 0.6 nm) supported on ZIF-8 surface whilst keeping the host framework intact.

(b) The catalytic employment of dehydrated RuNPs/ZIF-8 was firstly demonstrated in the catalytic dehydrogenation of DMAB in toluene at 40 °C, in which they provide high activity ($TOF_{initial} = 59\ min^{-1}$). The preliminary mechanistic studies done by ^{11}B NMR monitoring of the reaction solution revealed that the RuNPs/ZIF-8 catalyzed dehydrogenation of DMAB occurs in two different mechanisms yielding the final product through two different intermediates ($((CH_3)_2N{=}BH_2$ and $[(CH_3)_2NH\text{-}BH_2\text{-}N(CH_3)_2\text{-}BH_3]$) in toluene at 40 °C. Additionally, they show high stability against to leaching and agglomeration that makes them highly reusable catalyst (>85% activity at 5th run) in the dehydrogenation of DMAB.

(c) RuNPs/ZIF-8 was also used as catalyst in transfer hydrogenation of unsaturated hydrocarbons using DMAB as H_2 source. The efficient transfer hydrogenation of alkene/alkyne substrates using RuNPs/ZIF-8 as catalyst and DMAB as H_2 source presents an improvement in terms of safety with the elimination of the risks intrinsic to the transport and manipulation of the explosive compressed hydrogen gas.

Acknowledgements

MZ thanks to Yüzüncü Yıl University (BAP-2013-FEN-B015) for the financial support to his research laboratory. Additionally, the partial supports by Fevzi Akkaya Scientific Activities Support Fund (FABED), Science Academy and Turkish Academy of Sciences (TUBA) are gratefully acknowledged.

Appendix A. Supplementary data

Supplementary data associated with this article can be found, in the online version, at http://dx.doi.org/10.1016/j.apcatb.2014.06.009.

References

[1] A. Staubitz, A. Robertson, I. Manners, Chem. Rev. 110 (2010) 4079.
[2] A. Staubitz, A.P.M. Robertson, M.E. Sloan, I. Manners, Chem. Rev. 110 (2010) 4023.
[3] J. Turner, Science 285 (1999) 687.
[4] L. Schlaphach, A. Zuttel, Nature 414 (2001) 353.
[5] G.A. Deluga, J.R. Salge, L.D. Schmidt, X.E. Verykios, Science 303 (2004) 993.
[6] S. Karahan, M. Zahmakiran, S. Özkar, Chem. Commun. 48 (2012) 1180.
[7] A. Staubitz, P.A. Soto, I. Manners, Angew. Chem. 120 (2008) 6308.
[8] C.A. Jaska, I. Manners, J. Am. Chem. Soc. 126 (2004) 2698.
[9] C.E. Hartmann, V. Jurcık, O. Songis, C.S.J. Cazin, Chem. Commun. 49 (2013) 1005.
[10] Y. Jiang, H. Berke, Chem. Commun. (2007) 3571.
[11] J.G. de Vries, C.J. Elsevier, Handbook of Homogeneous Hydrogenation, Wiley-VCH, Weinheim, 2007.
[12] M. Zahmakiran, S. Özkar, Nanoscale 3 (2011) 3462.
[13] S. Özkar, R.G. Finke, J. Am. Chem. Soc. 124 (2002) 5796.
[14] M. Zahmakiran, S. Özkar, Sustainable Preparation of Metal Nanoparticles, RSC, London, 2013, p. 34.
[15] J.Y. Lee, O.K. Farha, J. Roberts, K.A. Scheidt, S.T. Nguyen, J.T. Hupp, Chem. Soc. Rev. 38 (2009) 1450.
[16] A. Corma, H. Garcia, F.X.L. Xamena, Chem. Rev. 110 (2010) 4606.
[17] K.S. Park, Z. Ni, A.P. Côté, J.Y. Choi, R. Huang, F.J. Uribe-Romo, H.K. Chae, M. O'Keeffe, O.M. Yaghi, Proc. Natl. Acad. Sci. U.S.A. 103 (2006) 10186.
[18] M. Zahmakiran, Dalton Trans. 41 (2012) 12690.
[19] H.L. Jiang, B. Liu, T. Akita, M. Haruta, H. Sakurai, Q. Xu, J. Am. Chem. Soc. 131 (2009) 11302.
[20] H.L. Jiang, T. Akita, T. Ishida, M. Haruta, Q. Xu, J. Am. Chem. Soc. 133 (2011) 1304.
[21] P.-Z. Li, K. Aranishi, Q. Xu, Chem. Commun. 48 (2012) 3173.
[22] T.T. Dang, Y. Zhu, J.S.Y. Ngiam, S.C. Ghosh, A. Chen, A.M. Seayad, ACS Catal. 3 (2013) 1406.
[23] P. Wang, J. Zhao, X. Li, Y. Yang, Q. Yang, C. Li, Chem. Commun. 49 (2013) 3330.
[24] D. Esken, H. Noei, Y. Wang, C. Wiktor, S. Turner, G. Van Tendeloo, R.A. Fischer, J. Mater. Chem. 21 (2011) 5907.
[25] C. Wagner, W.M. Riggs, L.E. Davis, J.F. Moulder, G.E. Muilenberg, Handbook of X-ray Photoelectron Spectroscopy, vol. 55, Physical Electronic Division, Perkin-Elmer, Eden Prairie, MN, 1979.
[26] R. Nyholm, N. Maartensson, Solid State Phys. 13 (1980), L279N.
[27] S. Storck, H. Bretinger, W.F. Maier, Appl. Catal. A 174 (1998) 137.
[28] R.S.H. Mikhail, S. Brunauer, E.E. Bodor, J. Colloid Interface Sci. 26 (1968) 45.
[29] W. Chen, D. Ghosh, J. Sun, M.C. Tong, F. Deng, S. Chen, Electrochim. Acta 63 (2007) 1150.
[30] M. Gulcan, M. Zahmakiran, S. Özkar, App. Cat. B: Env. 147 (2014) 394.
[31] M. Zahmakiran, S. Özkar, Inorg. Chem. 48 (2009) 8955.
[32] S. Çalışkan, M. Zahmakiran, F. Durap, S. Özkar, Dalton Trans. 41 (2012) 4976.
[33] M. Zahmakiran, M. Tristany, K. Philippot, K. Fajerwerg, S. Özkar, B. Chaudret, Chem. Commun. 46 (2010) 2938.
[34] M. Zahmakiran, K. Philippot, S. Özkar, B. Chaudret, Dalton Trans. 41 (2012) 590.
[35] R.J. Keaton, J.M. Blacquiere, R.T. Baker, J. Am. Chem. Soc. 129 (2007) 1844.
[36] J.R. Vance, A.P.M. Robertson, K. Lee, I. Manners, Chem. Eur. J. 17 (2011) 4099.
[37] G.R. Whittell, E.I. Balmond, A.P.M. Robertson, S.K. Patra, M.F. Haddow, I. Manners, Eur. J. Inorg. Chem. 3967 (2010).
[38] C.J. Stevens, R. Dallanegra, A.B. Chaplin, A.S. Weller, S.A. MacGregor, B. Ward, D. McKay, G. Alcaraz, S. Sabo-Etienne, Chem. Eur. J. 17 (2011) 3011.
[39] D.J. Liptrot, M.S. Hill, M.F. Mahon, D.J. MacDougall, Chem. Eur. J. 16 (2010) 8508.
[40] Y. Chen, J.L. Fulton, J.C. Linehan, T.J. Autrey, Am. Chem. Soc. 127 (2005) 3254.
[41] T.M. Douglas, A.B. Chaplin, A.S. Weller, X. Yang, M.B. Hall, J. Am. Chem. Soc. 131 (2009) 15440.
[42] A. Friedrich, M. Drees, S. Schneider, Chem. Eur. J. 15 (2009) 10339.
[43] B. Yang, X.-Q. Gong, H.-F. Wang, X.-M. Cao, J.J. Rooney, P. Hu, J. Am. Chem. Soc. 135 (2013) 15244.
[44] M. Poliakoff, J.M. Fitzpatrick, T.R. Farren, P.T. Anastas, Science 297 (2002) 807.